scientific reports

OPEN

Synthesis, biological evaluation and molecular modeling studies of methyl indole-isoxazole carbohydrazide derivatives as multi-target anti-Alzheimer's agents

Aida Iraji[1,2], Parisa Nikfar[3], Mohammad Nazari Montazer[4], Mona Karimi[5], Najmeh Edraki[6], Mina Saeedi[7,8]✉ & Seyedeh Sara Mirfazli[3]✉

Alzheimer's disease (AD) is a progressive neurodegenerative disorder that affects the elderly population globally and there is an urgent demand for developing novel anti-AD agents. In this study, a new series of indole-isoxazole carbohydrazides were designed and synthesized. The structure of all compounds was elucidated using spectroscopic methods including FTIR, ^{1}H NMR, and ^{13}C NMR as well as mass spectrometry and elemental analysis. All derivatives were screened for their acetylcholinesterase (AChE) and butyrylcholinesterase (BuChE) inhibitory activity. Out of all synthesized compounds, compound 5d exhibited the highest potency as AChE inhibitor with an IC_{50} value of 29.46 ± 0.31 μM. It showed significant selectivity towards AChE, with no notable inhibition against BuChE. A kinetic study on AChE for compound 5d indicated a competitive inhibition pattern. Also, 5d exhibited promising BACE1 inhibitory potential with an IC_{50} value of 2.85 ± 0.09 μM and in vitro metal chelating ability against Fe^{3+}. The molecular dynamic studies of 5d against both AChE and BACE1 were executed to evaluate the behavior of this derivative in the binding site. The results showed that the new compounds deserve further chemical optimization to be considered potential anti-AD agents.

Alzheimer's disease (AD) is a prevalent neurodegenerative condition which has been recognized as the primary cause of dementia in the world[1]. Its incidence is projected to affect 1 in 85 individuals globally by 2050. AD is categorized into two types based on age of onset and genetic factors: early-onset AD and late-onset AD. The latter constitutes more than 95% of all cases[2]. Several factors are known to increase the risk of AD, such as genetic, head injuries, vascular diseases, infections, and environmental factors; however, age is considered the most important risk factor[3]. The pathogenesis of AD is complex and involves multiple factors. It is characterized by accumulating extracellular amyloid-β (Aβ) plaques and intracellular neurofibrillary tangles. Additionally, oxidative stress

[1]Department of Persian Medicine, School of Medicine, Research Center for Traditional Medicine and History of Medicine, Shiraz University of Medical Sciences, Shiraz, Iran. [2]Stem Cells Technology Research Center, Shiraz University of Medical Sciences, Shiraz, Iran. [3]Department of Medicinal Chemistry, School of Pharmacy, Iran University of Medical Sciences, Tehran, Iran. [4]Endocrinology and Metabolism Research Center, Endocrinology and Metabolism Clinical Sciences Institute, Tehran University of Medical Sciences, Tehran, Iran. [5]Department of Chemistry, North Tehran Branch, Islamic Azad University, Tehran, Iran. [6]Medicinal and Natural Products Chemistry Research Center, Shiraz University of Medical Sciences, Shiraz, Iran. [7]Medicinal Plants Research Center, Faculty of Pharmacy, Tehran University of Medical Sciences, Tehran, Iran. [8]Persian Medicine and Pharmacy Research Center, Tehran University of Medical Sciences, Tehran, Iran. ✉email: m-saeedi@tums.ac.ir; saramirfazli@gmail.com; mirfazli.s@iums.ac.ir

and mitochondrial dysfunction play significant roles in the disease progression. These processes lead to the loss of synapses and neuronal death, resulting in decreased levels of the acetylcholine (ACh) neurotransmitter. Consequently, individuals experience cognitive decline and memory loss[3–5].

The neurotransmitter acetylcholine (ACh) in the brain is regulated by two enzymes, acetylcholinesterase (AChE) and butyrylcholinesterase (BChE). Among these, AChE plays the most significant role in AD progression and is considered an ideal target for "cholinergic dysfunction"[6,7]. As a result, acetylcholinesterase inhibitors such as donepezil, rivastigmine, and galantamine have been approved for clinical use and ongoing clinical trials are investigating more cholinesterase inhibitors[8].

The accumulation of Aβ plaques or senile plaques in the brain's extracellular region is linked to synaptic dysfunction, inflammatory responses, and neuronal loss. The formation of Aβ fibrils results from proteolytic cleavage of the amyloid precursor protein by the enzyme β-site APP cleaving enzyme 1 (BACE1), followed by γ-secretase action. Considering that BACE1 plays a crucial role in the pathogenesis of AD, the development of novel BACE1 inhibitors appears to be a logical approach for targeting the AD pathway[3]. This strategy has led to the design of drug candidates showing promising results in animal models[9,10].

Metal dyshomeostasis is another proposed mechanism of AD in which metal ions like Fe^{3+} participate in the peptide aggregations and misfolding mechanisms, leading to reactive oxygen species (ROS) generation and oxidative stress. In this context, metal chelating agents that can modulate the aggregation pathways are of great interest[11].

Indole and its derivatives are promising scaffolds that are ubiquitous in both synthetic and naturally-occurring compounds[12]. They possess various biological activities such as potent AChE[13] and tyrosinase[14] inhibitory activity as well as antibacterial[15], amoebicidal,[16] and anti-cancer effect[17]. Also, they have been important in the development of anti-AD drug candidates[18]. The presence of indole moiety is known to enhance the blood–brain barrier (BBB) penetration. 3-Indolepropionic acid and indole-3-propionamide are the two naturally occurring indoles showing potent neuroprotective activities at least twice as potent as melatonin in neutralizing free radicals[19]. Also, isoxazoles are within the wide range of heterocycles and substituted isoxazoles have been documented for their considerable biological activities[20]. Different studies have indicated the neuroprotective, anti-inflammatory, and antioxidant potential of isoxazole-based derivatives[21–23].

The fact that the pathogenesis of AD participates in multiple mechanisms has inspired researchers to develop multitarget-directed ligands (MTDLs) that can target these mechanisms simultaneously. The current study developed MTDLs containing indole-isoxazole scaffold as ChEs and BACE1 inhibitors with metal chelating ability. Also, the kinetic analysis and molecular dynamics simulation of the most potent compounds against the proposed targets were executed to study the behavior and key interactions of these derivatives within the binding site of enzymes.

Results and discussion
Chemistry
In this study, a novel series of indole-isoxazole-based Schiff bases were synthesized by the chronological reaction sequence depicted in Fig. 1. 1-(1-Methyl-1H-indol-3-yl)ethanone (**1**) was synthesized by the reaction of 3-acetylindole and methyl iodide in DMF in the presence of K_2CO_3 at 80 °C for 1.5 h. Ethyl 4-(1-methyl-1H-indol-3-yl)-2,4-dioxobutanoate (**2**) was accordingly prepared by dropwise addition of a mixture of diethyl oxalate/sodium ethoxide into the ethanolic solution of compound **1**. Then, the reaction of compound **2** and hydroxylamine hydrochloride in refluxing ethanol for 2 h led to the formation of the isoxazole ester derivative **3**[24], which tolerated the reaction with hydrazine hydrate in ethanol at 50 °C for 5 h to give compound **4**. Finally, products **5** (43–83%) were afforded by the reaction of desired benzaldehydes and compound **4** in the refluxing
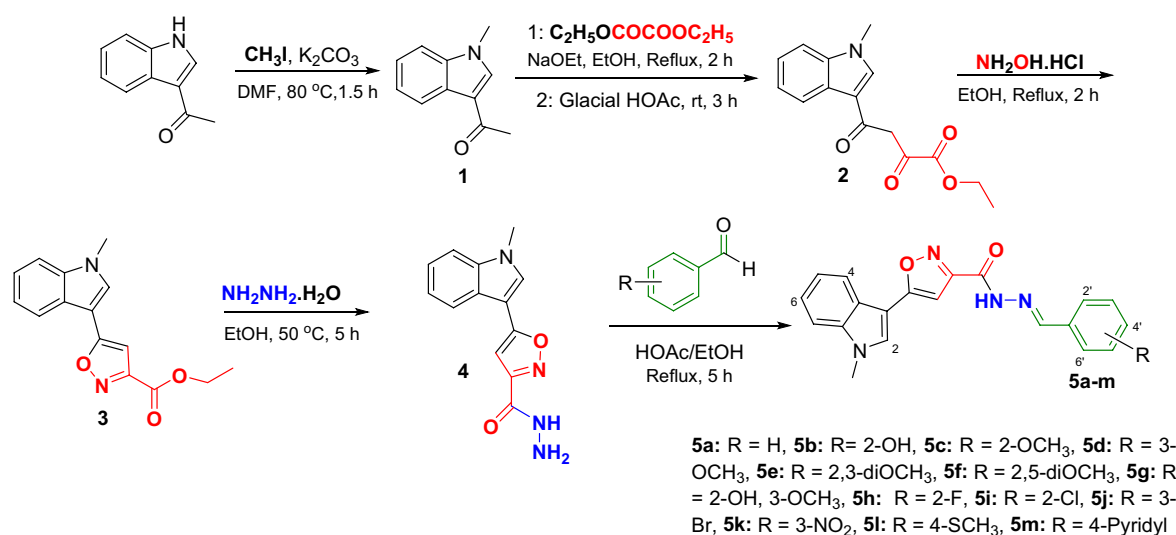
**Fig. 1.** The synthetic route for the preparation of compounds **5a–m**.

mixture of AcOH/H$_2$O for 5 h[25]. The structure of compounds was confirmed using ^{1}H NMR, ^{13}C NMR, and FT-IR spectroscopy as well as mass spectrometry and elemental analysis (supplementary figures).

Designing

Donepezil (**A**, Fig. 2) is known as an approved AChE inhibitor with similar behavior of ACh neurotransmitter in the active site of AChE. To design ChE inhibitors, the indanone moiety of donepezil was bioisosterically replaced with indole pharmacophore, and several indole–based derivatives were reported as effective cholinesterase inhibitors with memory-enhancing potential. It was shown that the indole moiety of the compound **B** participated in interaction with Trp84 of the peripheral anionic site (PAS) of AChE and provided a good fit to the binding site while the amide linker participated in critical H-bonding interactions with Phe121 and Phe288 of AChE active site[26]. *N*-substituted 2-aryl indole derivatives (e.g. compound **C**) were synthesized utilizing Suzuki–Miyaura cross-coupling reaction and screened for their activity to inhibit AChE and BuChE. All compounds exhibited significant selectivity and potency against AChE with IC$_{50}$ values in the range of 0.27 ± 0.01 to 21.5 ± 1.07 μM[27]. Structure–activity relationships (SARs) exhibited electron-donating groups were proven to increase effectiveness. Also, there are some reports about the neuroprotectivity and BACE1 inhibitory potential of indole derivatives[28,29]. On the other hand, indole enhances cholinesterase inhibition by lodging in the PAS and prevents AChE-induced Aβ aggregation.

The isoxazole nucleus is a valuable fragment with diverse pharmacological potencies as an anti-inflammatory, anticancer, antimicrobial, antidepressant and anticonvulsant agent[30]. New harmine-isoxazoles (e.g. compound **D**) were designed, and the most potent derivative demonstrated good potency compared with galantamine as a positive control with an IC$_{50}$ value of 4.1 ± 0.2 μM against AChE[23]. Recently, conjugation of indole with isoxazole derivatives (e.g. compound **E**) was reported as a ChE inhibitor and the molecular docking study of the most potent compound showed the vital role of indole moiety to interact with Phe330 and Phe331 amino acid residues and isoxazole ring exhibited H-bonding interaction with Gly117[31].

Regarding the multifactorial nature of AD, MTDLs that can mediate in the different pathological pathways have become a leading strategy for managing AD. As a result, herein molecular hybridization strategy was applied by incorporating indole into the isoxazole-carbohydrazide derivatives. This Schiff base linker is a key functionality that can participate in H-bonding interactions with the active site residues of the ChE enzymes and provide a suitable site for derivatization. All derivatives were evaluated as AChE and BuChE inhibitors and selected derivatives were assessed as possible BACE1 inhibitors. Next, metal chelation ability and kinetic study of the most potent derivative were executed.
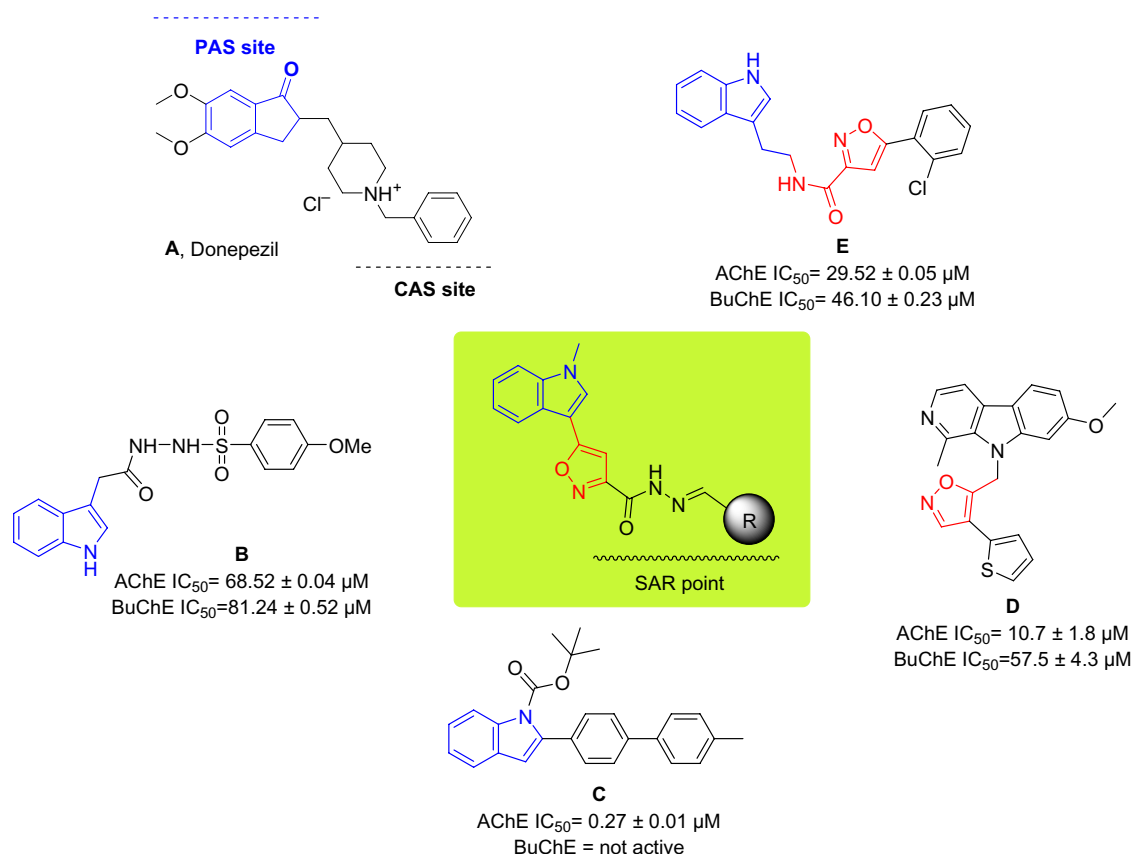
Fig.2. Design of the target methyl indole-isoxazole carbohydrazides.

In vitro biological assays

ChE inhibitory activity and SAR analysis

The effect of the indole-isoxazole derivatives bearing different carbohydrazide moiety against ChEs was investigated, compared with donepezil and rivastigmine as the reference drugs (Table 1).

The unsubstituted derivative (**5a**) exhibited no inhibitory potencies against both AChE and BuChE. Evaluation of compounds having electron-donating groups showed that 2-OH substitution (**5b**) did not improve the potency; however, the replacement of 2-OH with 2-OMe (**5c**) significantly enhanced the activity against AChE. Changing the position from *ortho* (**5c**) to *meta* (**5d**) resulted in the most effective inhibitor against the AChE with an IC_{50} value of 29.46 ± 0.31 μM. On the other hand, the AChE inhibitory activity of multi-substitution derivatives, including 2,3-diOMe (**5e**) and 2,5-diOMe (**5f**) deteriorated compared to their mono-substituted counterparts. Unexpectedly, 2-OH-3-OMe moiety recorded good inhibition with an IC_{50} value of 63.82 ± 4.04 μM. Next, the effect of electron-withdrawing groups against AChE inhibition was assessed, and **5h** (R = 2-F), **5i** (R = 2-Cl), and **5j** (R = 3-Br) exhibited no potency. The exception in this trend was the strong electron-withdrawing group NO_2 (**5k**, $IC_{50} = 45.57$ μM) that enhanced the activity compared with the rest of the electron-withdrawing groups. Finally, the replacement of benzyl moiety with pyridine did not increase the potency.

Assessments of BuChE inhibition exhibited that just compounds **5b** and **5k** bearing 2-OH and 3-NO_2 moieties inhibited BChE with IC_{50} values of 92.75 ± 2.29 and 71.31 ± 0.76 μM, respectively.
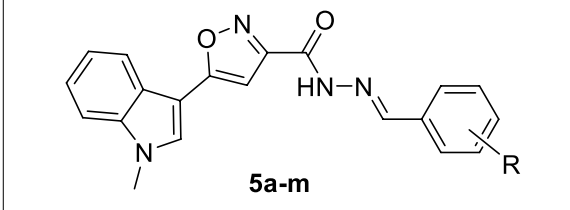
Overall, it can be understood that these derivatives were more potent against AChE than BuChE. Among different types of substitution against AChE, the methoxy group was the best choice, and the optimum position was meta.

Kinetic study on the inhibition of AChE by compound 5d

The mechanism of action of compound **5d** as the most potent AChE inhibitor was investigated towards the enzyme. According to the Lineweaver–Burk graph (Fig. 3a), K_m gradually increased, and V_{max} remained unchanged with increasing the concentration of **5d**, which indicated the competitive inhibition manner. In this respect, compound **5d** competes with the substrate for binding at the active site of the AChE by the formation of AChE-inhibitor complex. Also, the inhibitory constant (K_i) was calculated as 19.33 μM (Fig. 3b).

BACE1 inhibitory activity of selected derivatives

The inhibitory activity of the selected indole-isoxazoles on BACE1 was investigated and compared with OM99-2 ($IC_{50} = 0.014 \pm 0.003$ μM) as a positive control (Table 2). The best BACE1 inhibitory potency came back to derivative **5j** bearing 3-bromine as the halogen-substituted group with IC_{50} value of 1.99 ± 0.15 μM followed by mono electron donating moieties, **5b** (R = OH; $IC_{50} = 2.79 \pm 0.52$ μM) and **5d** (R = 3-OMe; $IC_{50} = 2.85 \pm 0.09$ μM).

Compound	R	AChE IC_{50} (μM)	BuChE IC_{50} (μM)
5a	H	> 100	> 100
5b	2-OH	> 100	92.75 ± 2.29
5c	2-OMe	34.19 ± 1.69	> 100
5d	3-OMe	29.46 ± 0.31	> 100
5e	2,3-DiOMe	> 100	> 100
5f	2,5-DiOMe	> 100	> 100
5g	2-OH-3-OMe	63.82 ± 4.04	> 100
5h	2-F	> 100	> 100
5i	2-Cl	> 100	> 100
5j	3-Br	> 100	> 100
5k	3-NO_2	45.57 ± 4.30	71.31 ± 0.76
5l	4-SMe	> 100	> 100
5m	Pyridine	> 100	> 100
Rivastigmine[b]		11.07 ± 0.01	7.72 ± 0.02
Donepezil[b]		0.079 ± 0.002	5.19 ± 0.38

Table 1. AChE and BuChE inhibitory activities of compounds **5a-m**[a]. [a]Each value represents the mean ± SD (n = 3). [b]Positive control.
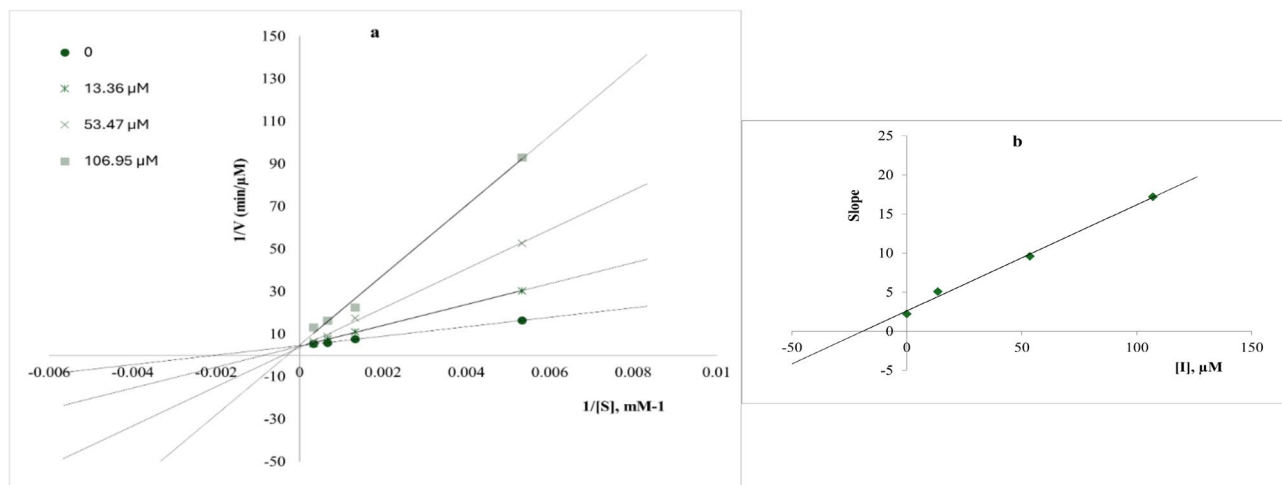
Fig.3. Kinetic study of AChE enzyme inhibition by compound **5d**.

Compound	R	IC$_{50}$ (µM)
5b	2-OH	2.79 ± 0.52
5d	3-OMe	2.85 ± 0.09
5e	2,3-DiOMe	8.28 ± 0.37
5i	2-Cl	13.42 ± 3.96
5j	3-Br	1.99 ± 0.15
5k	3-NO$_2$	> 100
5l	4-SMe	> 100
OM99-2		0.014 ± 0.003

Table 2. BACE1 inhibitory activities of selected derivatives[a]. [a]Each value represents the mean ± SD (n = 3)

2,3-DiOMe (**5e**) and chlorine substitution (**5i**) also recorded promising BACE1 inhibitory potential. However, nitro, a strong electron-withdrawing group with large dipole moments, and SMe showed inferior potency.

Metal chelating ability of compound 5d
Considering that 5d was a potent AChE and BACE1 inhibitor, its chelation ability was assessed by UV–visible spectrometry using Fe^{3+}. The spectra of **5d** indicated that there was no spectral shift in the presence of Fe^{3+} (Fig. 4), with the hyperchromic shift at 304 nm. The phenomenon showed that **5d** had biometal chelation ability.

Figure 5 illustrates the stoichiometric study of the Fe^{3+}-**5d** complex using the mole ratio test. Initially, the absorbance showed a linear increase, reaching a plateau after that. The intersection of the two straight lines occurred at a mole fraction of approximately 1, suggesting a 1:1 stoichiometry for the Fe^{3+}-**5d** complex.
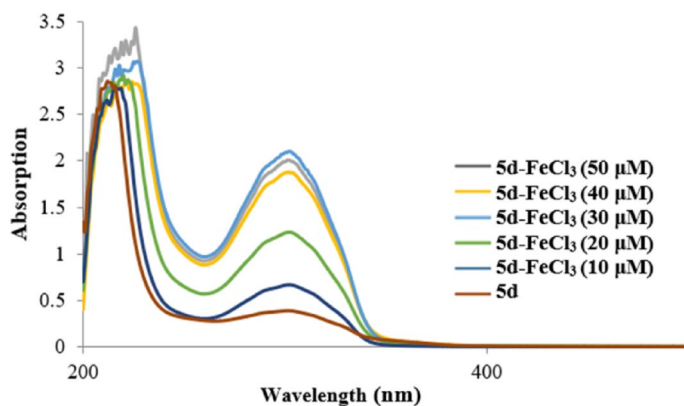
Fig.4. UV spectrum of **5d** alone or in the presence of different concentrations of FeCl$_3$.
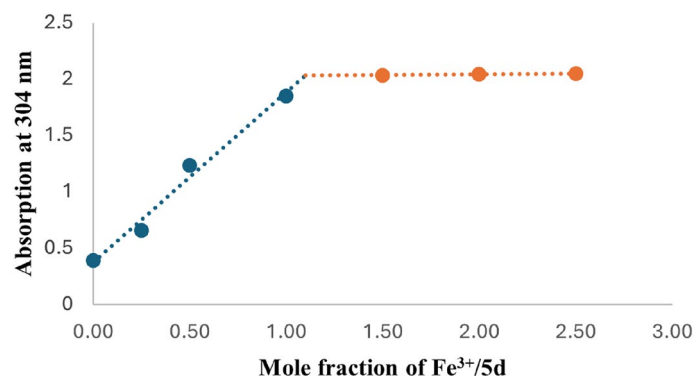
Fig.5. Determination of the stoichiometry of complex- Fe^{3+} using the molar ratio method through titrating the methanol solution of compound **5d** with ascending amounts of $FeCl_3$.

Molecular docking studies
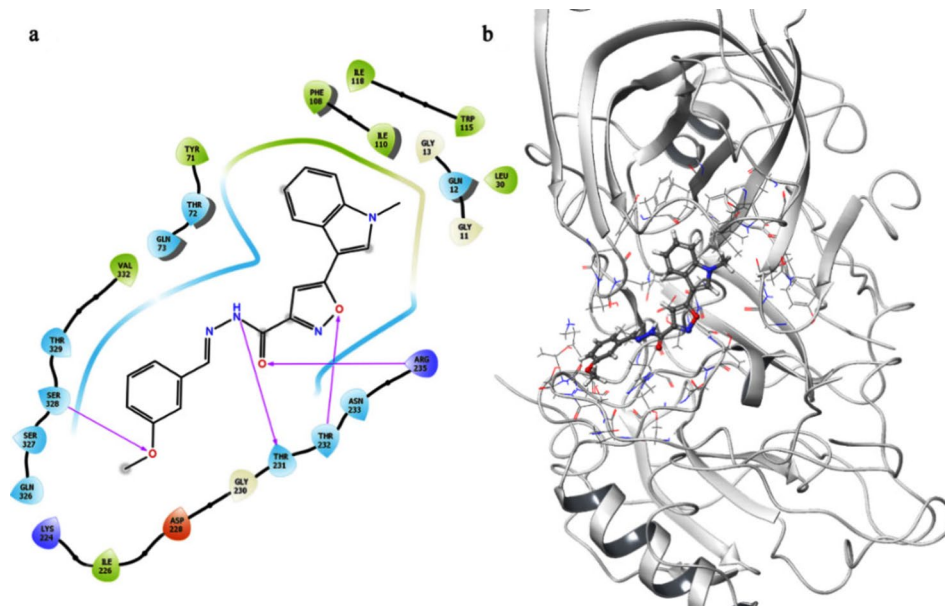
Molecular docking of 5d against AChE

The binding site of AChE comprises two parts. The PAS of AChE, which is at the mouth of the gorge, contains multiple aromatic side chains, including Tyr124, Tyr286, Phe295, Tyr337, and Phe338. The CAS of AChE consists of the catalytic triad Ser203, His447, and Glu334 and the anionic subsite, which can be found in the other part of AChE. Strong inhibitors require interactions with the mentioned residues. **5d**, the most potent compound against AChE, was chosen for in silico evaluations. As shown in Fig. 6, compound **5d** fitted well in the active site pocket of AChE, and H-bonding interaction was observed between the carbohydrazide linker and Trp124. Also, several pi-pi stacking interactions were observed between aromatic rings of the compound and Trp286.

Molecular docking study of 5d against BACE1

BACE1 is a transmembrane protein with an active site in the extracellular domain. The active site of BACE1 is spacious, comprising multiple subsites or pockets, designated as S1 to S4 and S1' to S4'. The central part of the active site is the S1' subsite, which contains the catalytic dyad comprising Asp32 and Asp238, along with two hydrophobic residues, Ile226 and Val332. β hairpin loop over the active site, known as the "flap" consists of residues 67 through 77. The molecular docking study used Maestro to predict the interaction mode of compound **5d** and the BACE1 enzyme (Fig. 7). The synthesized compound showed four hydrogen bonds with Ser328, Thr231, Thr232, and Arg235 residues. Many hydrophobic interactions were observed with Ile226, Val332, Tyr71, Phe108, Ile110, Ile118, Trp115, and Leu30 residues. The glide score for the best pose of the ligand was calculated to be -8.648 kcal/mol.
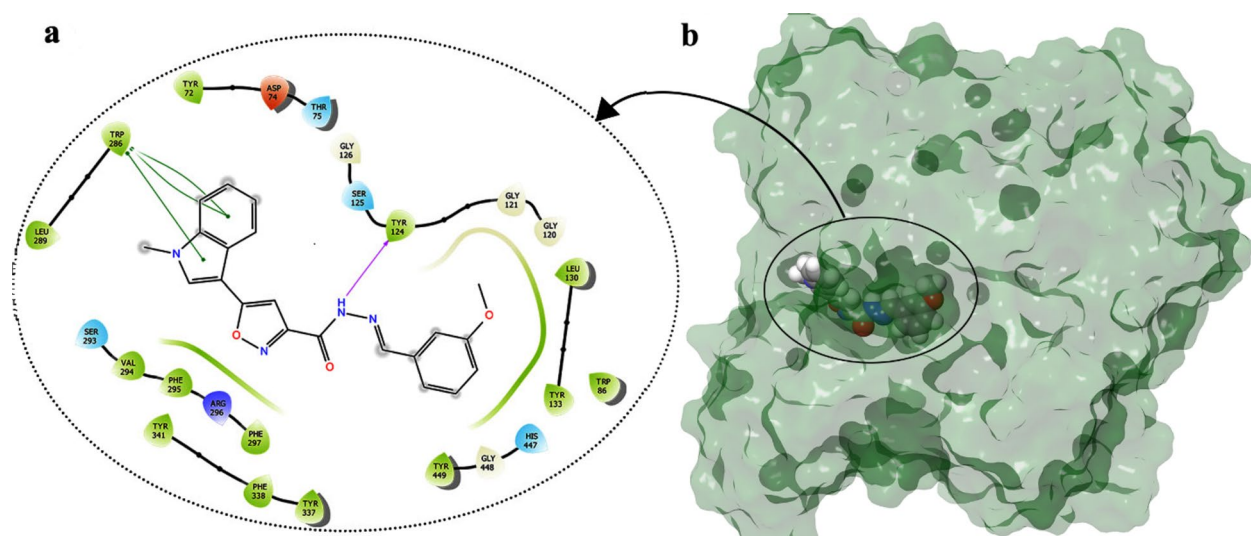
Fig. 6. (**a**) 2D presentation of compound **5d** interactions with active site pocket of AChE (**b**) 3D representation of **5d** interactions with the enzyme. (Desmond v5.3) https://www.schrodinger.com/life-science/download/release-notes/

Fig. 7. (**a**) 2D presentation of compound **5d** interactions with active site pocket of BACE1 (**b**) 3D representation of **5d** interactions with the enzyme. (Desmond v5.3) https://www.schrodinger.com/life-science/download/release-notes/

## Molecular dynamics studies

Molecular dynamics of 5d against AChE

The molecular docking study of compound **5d** in the AChE active site was repeated three times to gain better insight into the reproducibility of the results. The stability of the **5d**-AChE complex was examined by analyzing the root-mean-square deviation (RMSD). The RMSD of the system was evaluated at 310 K. It has been confirmed that an RMSD value of less than 3 Å indicates good stability. As shown in Fig. 8, in all replicates, the RMSD value was less than 2 Å, which is lower than that of AChE alone. This observation suggests that the introduction of **5d** enhances the stability of the complex.

Additionally, the root-mean-square fluctuation (RMSF) value measures the fluctuation of the protein's residues from their average position. According to Fig. 8, the N- and C-terminal tails fluctuate more than any other part of the protein. Furthermore, the ligand successfully participated in interactions with residues of the PAS pocket (Tyr72, Tyr74, Tyr124, Tyr341), the acyl pocket (Phe295, Arg296, Phe297), the choline-binding site (Trp86, Tyr337), and the catalytic triad (His447) of the enzyme.

The detailed interactions of compound **5d** with the enzyme are illustrated in Fig. 9. The indole ring forms a pi-pi stacking interaction with Arg296 in 35% to 52% of the simulation runs. The isoxazole moiety establishes a pi-pi stacking interaction with Tyr341 in all simulation runs, alongside a hydrogen bonding interaction with Phe295, occurring 93–97% of the simulation time. Moreover, the oxygen atom of the amide linker exhibits a strong hydrogen bonding interaction with Arg296 for a significant portion of the simulation time, while the NH moiety forms another hydrogen bond with Tyr124. Additionally, the benzylidene ring engages in two pi-pi stacking interactions with residues Trp86 and Tyr337. Furthermore, the terminal MeO group forms a hydrogen bonding interaction with His447.

Molecular dynamics of 5d against BACE1

The conformational stability of the protein–ligand complex trajectories was evaluated by calculating the backbone root-mean-square deviation (RMSD) throughout the molecular dynamics (MD) simulation (Fig. 10). The RMSD analysis is a critical metric for assessing the stability of the protein–ligand complex over time. In the case of the **5d**-BACE1 complex, the RMSD values were consistently lower compared to the apoenzyme in three different runs, indicating that the presence of compound **5d** enhances the stability of the BACE1 complex. The root-mean-square fluctuation (RMSF) of the Cα atoms provides insight into the flexibility and movement of individual amino acid residues within the protein. For the **5d**-BACE1 complex, a notable decrease in RMSF was observed, particularly in the amino acid sequences 70–90 of the flap region and 210–240 of the catalytic domains, which are recognized as part of the enzyme's binding pocket. This reduction in RMSF suggests that the binding of compound **5d** to BACE1 results in a more rigid and stable binding pocket. These results indicate that compound **5d** not only successfully interacts with BACE1 but also significantly reduces its fluctuation, thereby contributing to the stability of the enzyme's active site. The stabilization of these key regions within the binding pocket implies that **5d** effectively inhibits BACE1 by reducing the dynamic nature of the enzyme, which is crucial for its catalytic activity.
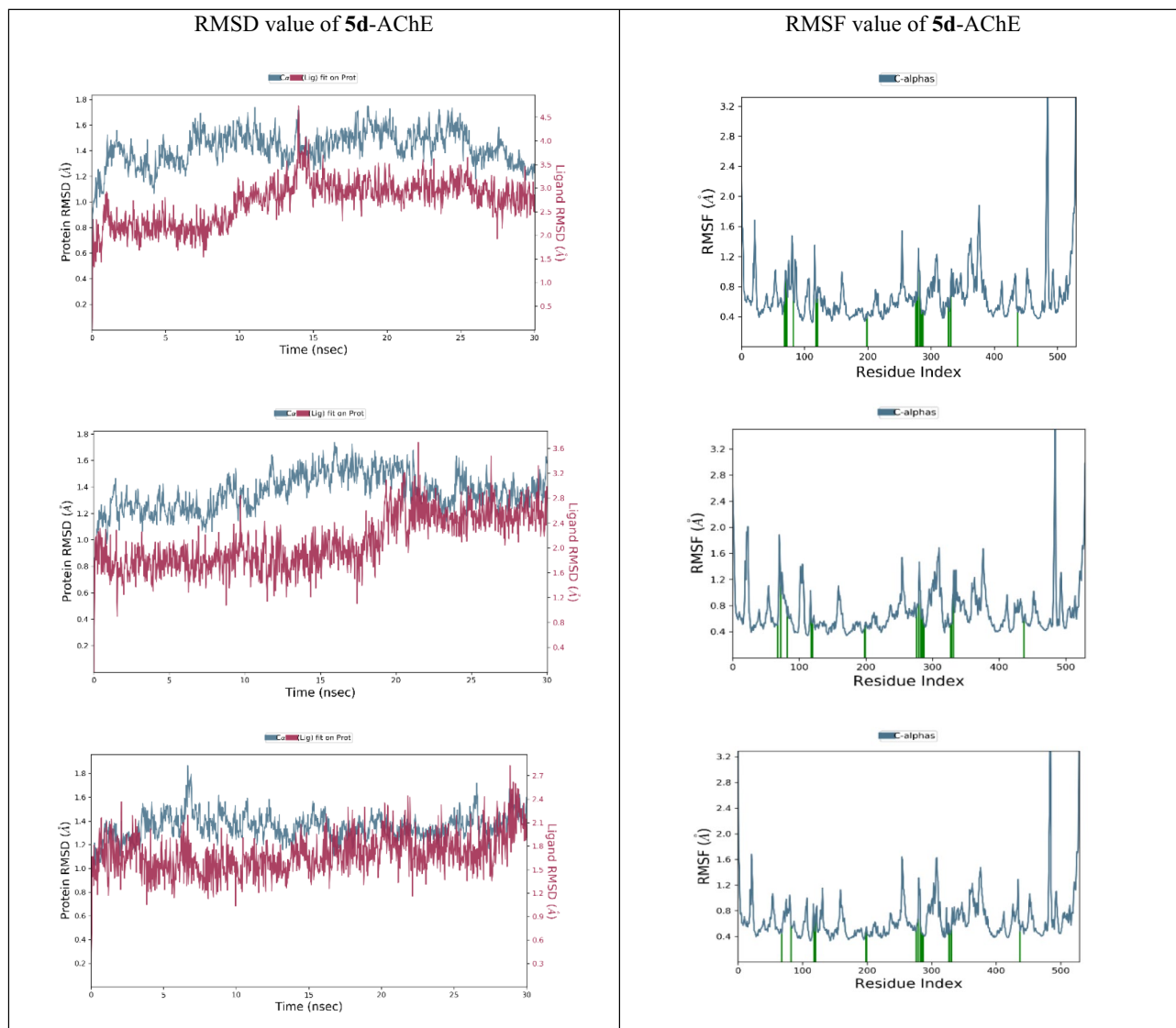
Fig. 8. The RMSD of the AChE enzyme in complex with compound **5d** (in red), and the unbound enzyme (in blue) and RMSF results of **5d**-AChE repeated three times.

Fig. 11 shows the molecular interactions between compound **5d** and the active site pocket of BACE1. The indole ring of compound **5d** recorded a pi-pi stacking interaction with Tyr71, which plays a crucial role in stabilizing the complex through aromatic interactions.

Additionally, a hydrogen bond interaction was observed between Thr72 and the NH linker of compound **5d**, further contributing to the stability and specificity of the binding. In some snapshots of the simulation, a hydrogen bonding interaction with Arg235 was also recorded, indicating dynamic yet significant interaction patterns. Moreover, interactions with Thr232 and Thr235 of the BACE1 active site were observed with the isoxazole ring of compound **5d**, showcasing multiple points of contact that enhance binding affinity and stability. The terminal methoxy group of compound **5d** formed another hydrogen bonding interaction with Ser328, indicating the extensive network of hydrogen bonding interactions that stabilize the ligand within the active site.

Conclusion

Regarding the multifactorial nature of AD, MTDLs seem more likely to achieve the therapy goals for AD. This study described the design and synthesis of indole-isoxazole carbohydrazide derivatives as anti-AD agents. All synthesized compounds were evaluated as possible ChE inhibitors, and the results showed that these derivatives were more potent against AChE than BuChE. The most potent compound, **5d**, exhibited an IC_{50} value of 29.46 ± 0.31 μM against AChE with no potency against BuChE. This derivative also recorded a K_i value of 19.33 μM in a competitive mode of inhibition. The iron-chelating potential of **5d** was confirmed using the mole ratio method. The in vitro BACE1 inhibitory potential of **5d** exhibited promising activity, with an IC_{50} value of 2.85 ± 0.09 μM. Molecular docking and molecular dynamic simulation showed that **5d** could bind to the active sites of both AChE and BACE1, further validating the rationality of the design strategy. These results suggested

Ligand atom interactions of **5d** with the protein	**5d**-AChE Type of contact during MD run
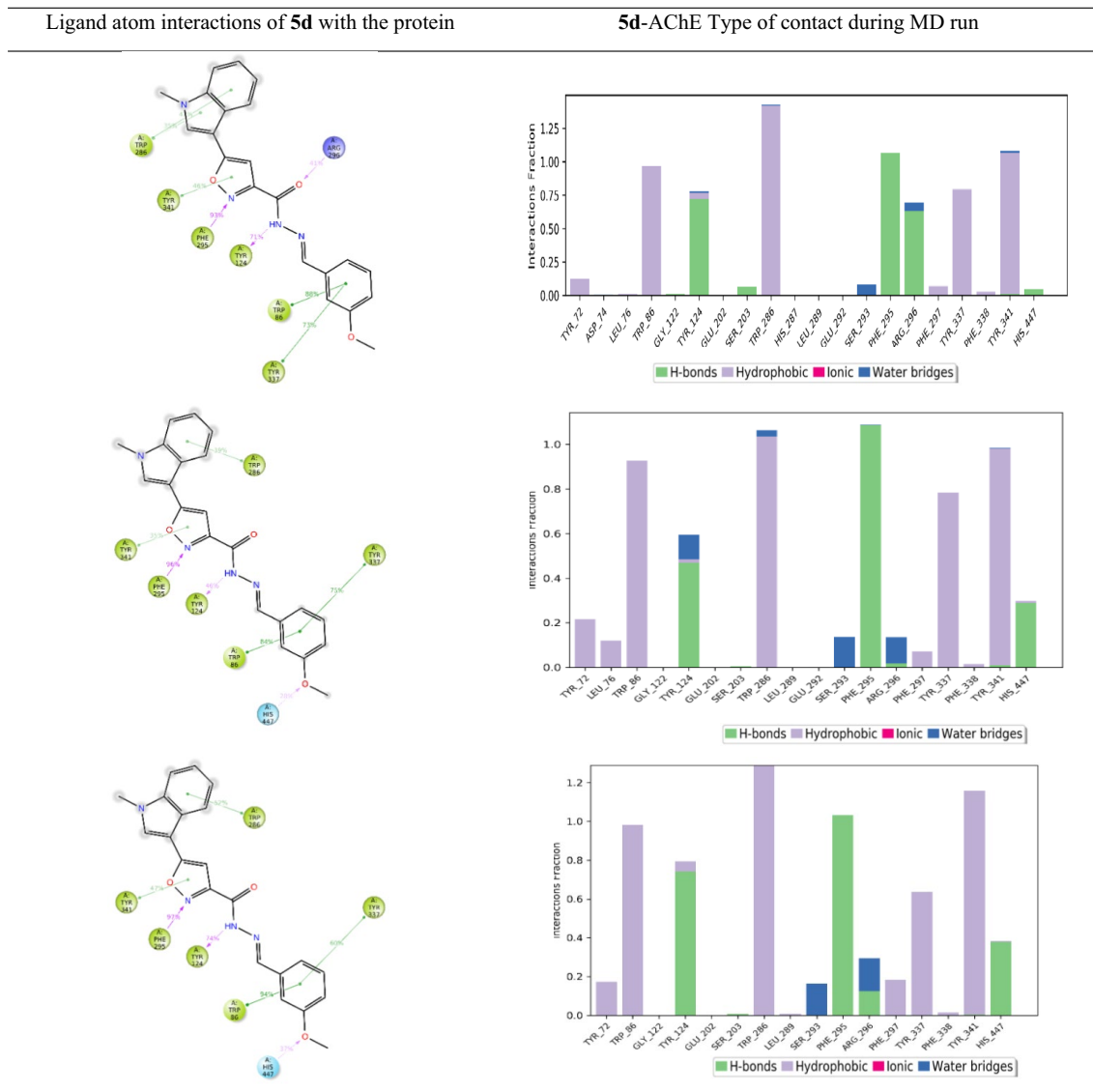
Fig. 9. The 2D representation of major interactions of compound **5d** with the active site pocket residues of AChE and type of ligand–protein contact.

that introducing an indole-isoxazole scaffold provided a useful template for developing potential chemical entities against AD.

Method and materials
Chemical and instruments
Organic chemicals and solvents were sourced from reputable companies and used without additional purification. Analytical TLC was conducted with pre-coated aluminum sheets and silica gel to check reaction completion and compound purity. Melting points were measured using an Electrothermal 9100 apparatus. ^{1}H NMR and ^{13}C NMR spectra were recorded on Bruker 400–500 MHz instruments with TMS as the internal standard and $CDCl_3$ and DMSO-d_6 as solvents. Elemental analysis for C, H and N was performed using a Costech model 4010 instrument, and the obtained values closely matched theoretical values within ± 0.4% deviation. Electrospray ionization mass spectra (ESI–MS) were obtained using Agilent 6410 Triple Quad. LC/MS. LC chromatograms were obtained using HPLC system (YL9100) equipped with UV detector, isocratic mobile phase was CH_3OH: H_2O (80:20 v/v).

Synthesis of 1-(1-methyl-1*H*-indol-3-yl)ethanone (1)
A mixture of 3-acetylindole (1.0 mmol) and K_2CO_3 (1.5 mmol) in DMF (5 ml) was stirred at room temperature for 15 min. After that the methyl iodide (1.1 mmol) was added and the reaction was stirred for 4 h at 80°C. The reaction mixture was added into ice-cold water, the precipitates were collected by filtration, and used for the next step without further purification. Yield: 81%; white crystals; m.p. 106–108 °C. FT-IR (KBr) cm^{-1}: 3114, 1676, 1261. ^{1}H NMR (500 MHz, CDCl$_3$-d_6): δ 8.36 (s, 1H, Indole H$_4$), 7.69 (s, 1H, −N = CH-), 7.32 (m, 3H, Indole H$_5$,

RMSD value of **5d**-BACE1   RMSF value of **5d**-BACE1
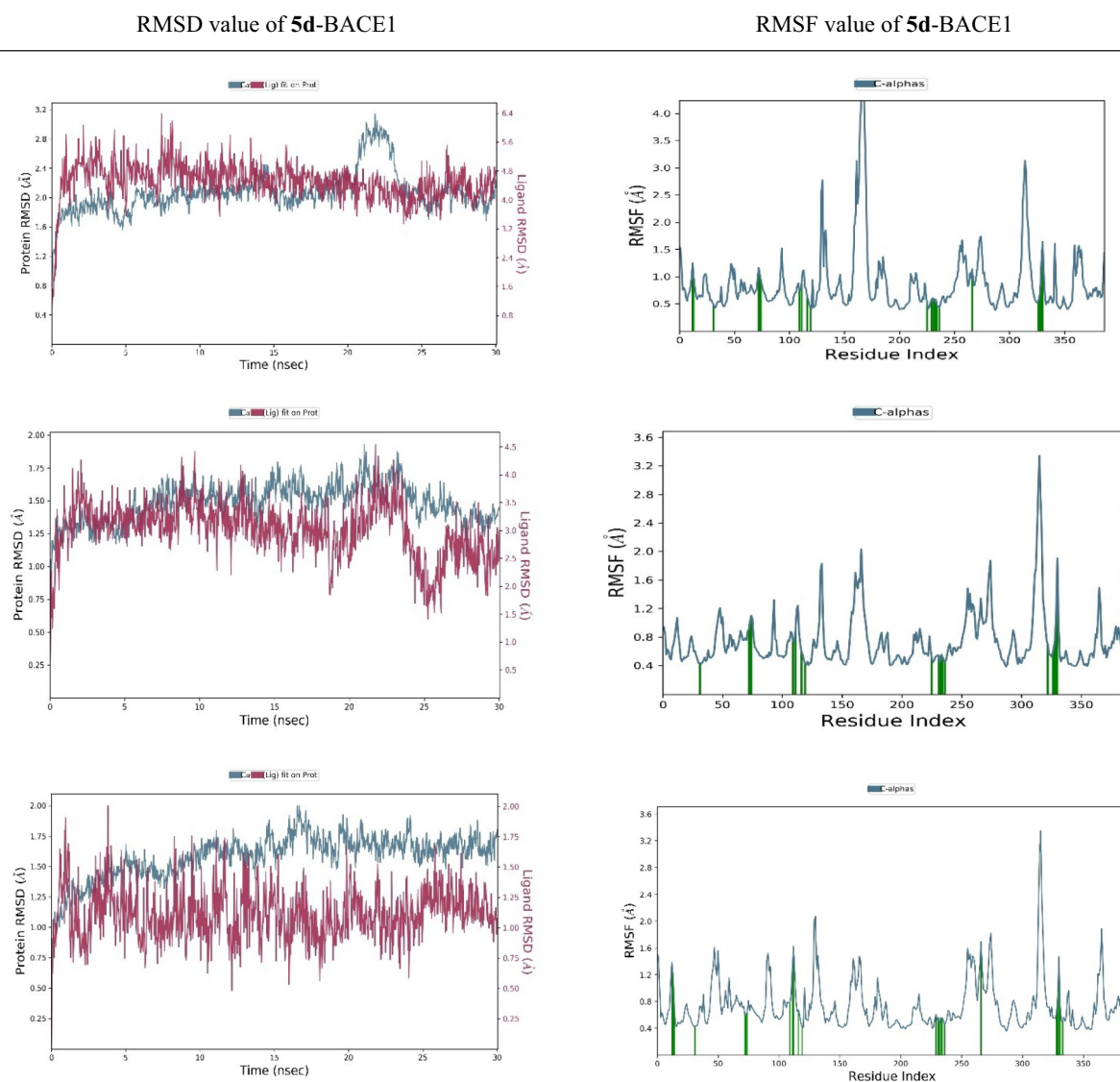
Fig. 10. The RMSD of the BACE1 enzyme in complex with compound **5d** (in red), and the unbound enzyme (in blue) and RMSF results of **5d**- BACE1 repeated three times.

H_6, H_7), 3.84 (s, 3H, N—CH_3), 2.52 (s, 3H, CH_3). ESI-Mass m/z: 174 $[M + H]^+$. Anal. Calcd. for $C_{11}H_{11}NO$: C, 76.28; H, 6.40; N, 8.09. Found: C, 75.97; H, 6.08; N, 8.32.

Synthesis of ethyl 4-(1-methyl-1*H*-indol-3-yl)-2,4-dioxobutanoate (2)

The mixture of freshly prepared NaEtO 10% (10 mL) and diethyloxalate (1.5 mmol) was added dropwise into the stirring compound **1** (1.0 mmol) in ethanol at 0 °C. Then, the reaction mixture was stirred at 75 °C for 2 h to appear orange precipitate. To quench the reaction, 2 mL glacial acetic acid (HOAc) was added and stirred for 3 h to give a yellow precipitate. After filtration, the precipitates were washed thoroughly with water and compound **2** was obtained. Yield: 81%; Yellow solid; m.p. 124- 125 °C. FT-IR (KBr) cm^{-1}: 3114, 2977, 2929, 1738. ^{1}H NMR (500 MHz, $CDCl_3$): δ 15.48 (bs, 1H, OH), 8.37 (d, 1H, $J = 6.8$ Hz, Indole H_4), 7.85 (s, 1H, Indole H_2), 7.37- 7.35 (m, 3H, Indole H_5, H_6, H_7), 6.84 (s, 1H, =CH—OH), 4.39 (q, 2H, $J = 7.0$ Hz, CH_2), 3.88 (s, 3H, CH_3), 1.42 (t, 3H, $J = 7.0$ Hz, CH_3).^{13}C NMR (125 MHz, DMSO-d_6): 189.0, 162.7, 162.2, 139.9, 138.3, 126.0, 124.1, 123.4, 122.1, 114.0, 111.7, 101.0, 62.3, 34.0, 14.4. ESI-Mass m/z: 274 $[M + H]^+$. Anal. Calcd. for $C_{15}H_{15}NO_4$: C, 65.92; H, 5.53; N, 5.13. Found: C, 65.68; H, 5.28; N, 5.40.

Synthesis of ethyl 5-(1-methyl-1*H*-indol-3-yl)isoxazole-3-carboxylate (3)

Compound **2** (1.0 mmol) reacted with hydroxylamine hydrochloride (1.0 mmol) in ethanol and the mixture was refluxed for 6 h. Then, the reaction was cooled and poured into the ice-cold water and the resulting pale green

Ligand atom interactions of **5d** with the protein	**5d**- BACE1; Type of contact during MD run
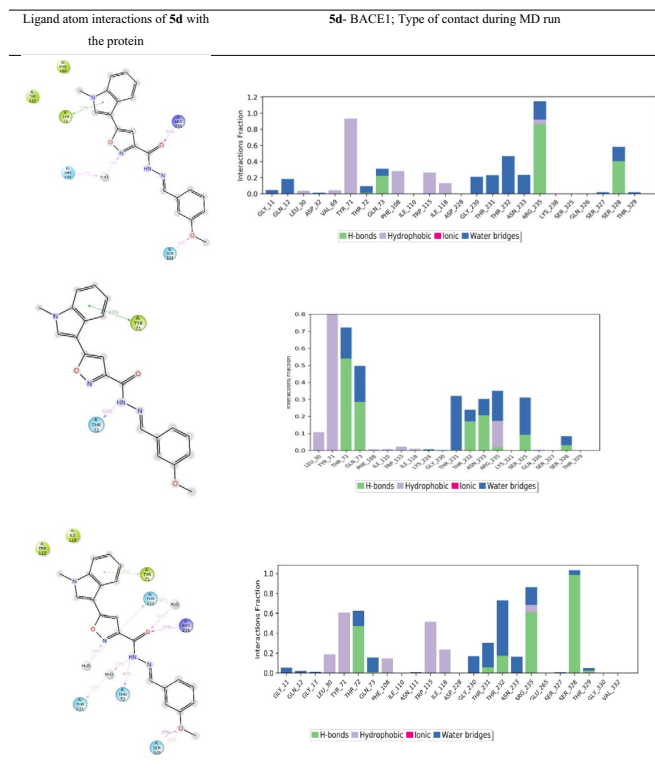
Fig. 11. The 2D representation of major interactions of compound **5d** with the active site pocket residues of BACE1 and type of ligand–protein contact.

precipitates (**3**) were collected after filtration. Yield: 95%; Pale-green solid; m.p: 141–143 °C. FT-IR (KBr) cm⁻¹: ν 3166, 3119, 1726 (C = O). ¹H NMR (500 MHz, DMSO-d_6): δ 8.21 (s, 1H, Indole H₂), 8.01 (d, 1H, J = 8.0 Hz, Indole H₄), 7.60 (d, 1H, J = 8.0 Hz, Indole H₇), 7.31 (dt, 2H, J = 24.0, 8.0 Hz, Indole H₅, H₆), 7.11 (s, 1H, Isoxazole), 4.40 (dd, 2H, J = 12.0, 8.0 Hz, CH₂), 3.90 (s, 3H, N−CH₃), 1.36 (t, 3H, J = 8.0 Hz, CH₃). ¹³C NMR (125 MHz, DMSO-d_6): 168.9, 160.2, 156.8, 137.4, 131.3, 124.3, 123.2, 121.9, 120.2, 111.4, 102.2, 97.5, 62.2, 33.5, 14.5. ESI-Mass m/z: 271 [M + H]⁺. Anal. calcd. for C₁₅H₁₄O₃N₂: C, 66.66; H, 5.22; N, 10.36. Found: C, 66.73; H, 5.56; N, 10.03.

Synthesis of 5-(1-methyl-1*H*-indol-3-yl)isoxazole-3-carbohydrazide (4)
To a solution of compound (**3**) (1.0 mmol) in ethanol, hydrazine monohydrate 95% (1.5 mmol) was added and stirred at 50 °C for 2 h. The mixture was cooled down by the addition of a water/ice mixture and compound **4** was collected by filtration. Yield: 81%; off-withe solid; m.p: 237- 239 °C. FT-IR (KBr) cm⁻¹: ν 3257.64 (NH), 1675.00, 1626.22. ¹H NMR (500 MHz, DMSO-d_6): δ 13.31 (s, 1H, CONH), 9.37 (s, 1H, Indole H₂), 7.87 (d, 1H, J = 8.0 Hz, Indole H₄), 7.78 (s, 1H, Isoxazole), 7.53 (d, 1H, J = 8.0 Hz Indole H₇), 7.26 (t, 1H, J = 8.0 Hz Indole H₅), 7.18 (t, 1H, J = 8.0 Hz Indole H₆), 4.42 (s, 2H, NH₂), 3.85 (s, 3H, CH₃). ¹³C NMR (125 MHz, DMSO-d_6): 165.2, 162.1, 149.1, 137.3, 128.0, 122.5, 121.1, 120.7, 119.8, 110.8, 104.5, 101.6, 33.2. ESI-Mass m/z: 257 [M + H]⁺. Anal. calcd. for C₁₅H₁₄N₄O₂: C, 60.93; H, 4.72; N, 21.86. Found: C, 61.22; H, 4.66; N, 22.13.

General procedure for the synthesis of compound 5a-m
A mixture of compound **4** (1.0 mmol) and the appropriate aromatic aldehydes (1.0 mmol) in the presence of a catalytic amount of glacial acetic acid (HOAc, 0.5 mL) was heated at reflux in the absolute ethanol for 4 h and then left to cool. The resulting precipitates were filtered, dried, and finally recrystallized from ethanol to afford desired compounds **5a-m**.

N′-Benzylidene-5-(1-methyl-1*H*-indol-3-yl)isoxazole-3-carbohydrazide (5a)
Yield: 57%; light-brown solid; m.p. 219–222 ℃. ¹H NMR (400 MHz, DMSO-d_6): δ 8.55 (s, 1H, CONH), 8.15 (bs, 1H, −N = CH−), 7.99–7.73 (m, 4H, −N = CH−C₆H₅ H₂, H₄, H₆, Indole H₂), 7.54–7.48 (m, 4H, Indole H₄, H₇, −N = CH−C₆H₅ H₃, H₅), 7.29–7.23 (m, 2H, Indole H₅, H₆), 7.08 (s, 1H, Isoxazole), 3.87 (s, 3H, N−CH₃). ¹³C NMR (100 MHz, DMSO-d_6): 166.6, 159.1, 149.9, 143.7, 139.0, 137.3, 136.0, 132.0, 131.0, 130.9, 126.5, 125.1, 123.1, 121.9, 120.1, 110.9, 102.6, 100.0, 98.5, 26.0. ESI-Mass m/z: 345 [M + H]⁺. Anal. calcd. for C₂₀H₁₆N₄O₂: C, 69.76, H, 4.68; N, 16.27. Found: C, 69.36; H, 4.91; N, 16.02.

N′-(2-Hydroxybenzylidene)-5-(1-methyl-1*H*-indol-3-yl)isoxazole-3-carbohydrazide (5b)

Yield: 43%; light-gray solid; m.p. 283–285 ℃. ^{1}H NMR (400 MHz, DMSO-d_6): δ 12.09 (s, 1H, CONH), 11.47 (s, 1H, −N = CH−), 9.01 (s, 1H, OH), 8.72 (s, 1H, −N = CH−C_6H_5 H_3), 7.90 (d, 1H, J = 8.0 Hz, Indole H_4), 7.85 (s, 1H, Indole H_2), 7.70 (d, 1H, J = 8.0 Hz, −N = CH−C_6H_5 H_5), 7.55 (d, 1H, J = 8.0 Hz, Indole H_7), 7.48 (d, 1H, J = 8.0 Hz, −N = CH−C_6H_5 H_6), 7.30 (m, 2H, Indole H_5, −N = CH−C_6H_5 H_4), 7.21 (t, 1H, J = 8.0 Hz, Indole H_6) 7.07 (s, 1H, Isoxazole), 3.88 (s, 3H, N−CH_3). ^{13}C NMR (100 MHz, DMSO-d_6): 167.5, 159.1, 158.2, 156.9, 149.7, 141.3, 138.2, 131.0, 129.4, 128.4, 123.2, 121.4, 120.0, 119.8, 117.9, 116.9, 110.1, 102.6, 98.2, 38.5. ESI-Mass m/z: 361 [M + H]$^+$. Anal. calcd. for $C_{20}H_{16}N_4O_3$: C, 66.66, H, 4.48; N, 15.55. Found: C, 66.32; H, 4.27; N, 15.74.

N′-(2-Methoxybenzylidene)-5-(1-methyl-1*H*-indol-3-yl)isoxazole-3-carbohydrazide (5c)

Yield: 61%; cream-white solid; m.p. 160–161 ℃. ^{1}H NMR (400 MHz, DMSO-d_6): δ 8.87 (s, 1H, CONH), 7.91–7.89 (m, 2H, −N = CH−, Indole H_4), 7.83 (s, 1H, Indole H_2), 7.72 (m, 1H, −N = CH−C_6H_5 H_6), 7.56–7.49 (m, 1H, −N = CH−C_6H_5 H_4), 7.47–7.34 (m, 2H, Indole H_5, H_7), 7.28–7.21 (m, 2H, −N = CH−C_6H_5 H_5, Indole H_6) 7.19–7.04 (m, 2H, −N = CH−C_6H_5 H_3, Isoxazole) 3.87 (s, 6H, CH_3). ^{13}C NMR (100 MHz, DMSO-d_6): 168.7, 159.5, 159.1, 150.9, 149.3, 139.2, 138.0, 137.9, 129.5, 128.9, 124.2, 123.8, 122.5, 121.6, 119.9, 110.7, 104.5, 101.7, 100.2, 56.9, 38.4. ESI-Mass m/z: 375 [M + H]$^+$. Anal. calcd. for $C_{21}H_{18}N_4O_3$: C, 67.37, H, 4.85; N, 14.96. Found: C, 67.02; H, 4.86; N, 15.14.

N′-(3-Methoxybenzylidene)-5-(1-methyl-1*H*-indol-3-yl)isoxazole-3-carbohydrazide (5d)

Yield: 83%; light-brown solid; m.p. 183–185 ℃. ^{1}H NMR (400 MHz, DMSO-d_6): δ 8.52 (s, 1H, CONH), 8.15 (bs, 1H, −N = CH−), 7.90 (d, 1H, J = 8.0 Hz, Indole H_4), 7.85 (s, 1H, Indole H_2), 7.56 (d, 1H, J = 8.0 Hz, Indole H_7), 7.39 (t, 1H, J = 8.0 Hz, Indole H_5), 7.30- 7.27 (m, 3H, Indole H_6, −N = CH−C_6H_5 H_2, H_6), 7.21 (t, 1H, −N = CH−C_6H_5 H_5), 7.06–7.01 (m, 2H, −N = CH−C_6H_5 H_4, Isoxazole), 3.88 (s, 3H, CH_3), 3.83 (s, 3H, N−CH_3). ^{13}C NMR (100 MHz, DMSO-d_6): 168.6, 159.0, 159.0, 149.7, 148.1, 144.7, 139.0, 138.1, 137.3, 134.8, 128.3, 127.9, 123.5, 120.0, 114.0, 110.5, 104.5, 102.1, 100.5, 56.7, 34.9. ESI-Mass m/z: 375 [M + H]$^+$. Anal. calcd. for $C_{21}H_{18}N_4O_3$: C, 67.37, H, 4.85; N, 14.96. Found: C, 67.52; H, 4.63; N, 15.24.

N′-(2,3-Dimethoxybenzylidene)-5-(1-methyl-1*H*-indol-3-yl)isoxazole-3-carbohydrazide (5e)

Yield: 69%; cream-white solid; m.p. 232–234 ℃. ^{1}H NMR (400 MHz, DMSO-d_6): δ 11.79 (s, 1H, CONH), 8.84 (s, 1H, −N = CH−), 7.91 (d, 1H, J = 8.0 Hz, Indole H_4), 7.85 (s, 1H, Indole H_2), 7.57 (d, 1H, J = 8.0 Hz, Indole H_7), 7.50 (d, 1H, J = 8.0 Hz, −N = CH−C_6H_5 H_6), 7.28 (t, 1H, J = 8.0 Hz, Indole H_5), 7.23 (t, 1H, J = 8.0 Hz, Indole H_6), 7.17–7.11 (m, 2H, −N = CH−C_6H_5 H_4, H_5), 7.07 (s, 1H, Isoxazole), 3.91 (s, 3H, CH_3), 3.88 (s, 3H, CH_3), 3.85 (s, 3H, N−CH_3). ^{13}C NMR (100 MHz, DMSO-d_6): 158.8, 153.2, 148.5, 146.9, 143.4, 139.1, 137.3, 128.3, 125.1, 124.8, 122.5, 120.7, 119.8, 119.4, 117.5, 114.5, 110.8, 104.0, 102.5, 61.7, 56.5, 33.3. ESI-Mass m/z: 405 [M + H]$^+$. Anal. calcd. for $C_{22}H_{20}N_4O_4$: C, 65.34, H, 4.98; N, 13.85. Found: C, 65.59; H, 5.30; N, 13.92.

N′-(2,5-Dimethoxybenzylidene)-5-(1-methyl-1*H*-indol-3-yl)isoxazole-3-carbohydrazide (5f)

Yield: 43%; off-white solid; m.p. 166–168 ℃. ^{1}H NMR (400 MHz, DMSO-d_6): δ 8.85 (s, 1H, CONH), 8.10 (s, 1H, −N = CH−), 7.90- 7.83 (m, 3H, Indole H_2, H_4, H_7), 7.72 (s, 1H, −N = CH−C_6H_5 H_6), 7.54–7.22 (m, 4H, Indole H_5, H_6, −N = CH−C_6H_5 H_3, H_4), 7.07 (s, 1H, Isoxazole), 3.84 (s, 3H, CH_3) 3.78 (s, 6H, CH_3, N−CH_3). ^{13}C NMR (100 MHz, DMSO-d_6): 169.5, 160.0, 157.1, 154.4, 152.0, 143.9, 137.8, 129.0, 128.0, 124.5, 121.7, 120.2, 118.8, 114.7, 112.8, 112.8, 109.7, 106.6, 98.8, 58.1, 0.54.8, 33.6. ESI-Mass m/z: 405 [M + H]$^+$. Anal. calcd. for $C_{22}H_{20}N_4O_4$: C, 65.34, H, 4.98; N, 13.85. Found: C, 65.21; H, 5.23; N, 13.47.

N′-(2-Hydroxy-3-methoxybenzylidene)-5-(1-methyl-1*H*-indol-3-yl)isoxazole-3-carbohydrazide (5g)

Yield: 54%; ligt-gray solid; m.p. 268–269 ℃. ^{1}H NMR (400 MHz, DMSO-d_6): δ 12.07 (s, 1H, −N = CH−C_6H_5 OH), 11.22 (s, 1H, CONH), 8.72 (s, 1H, −N = CH−), 7.90–7.83 (m, 2H, Indole H_2, H_4), 7.54 (d, 1H, J = 8.0 Hz, Indole H_7), 7.28–7.18 (m, 2H, Indole H_5, H_6), 7.09–7.03 (m, 2H, −N = CH−C_6H_5 H_4, H_6), 7.09 (s, 1H, Isoxazole), 6.88 (t, 1H, J = 8.0 Hz, −N = CH−C_6H_5 H_5), 3.87 (s, 3H, N−CH_3), 3.82 (s, 3H, CH_3). ^{13}C NMR (100 MHz, DMSO-d_6): 165.5, 154.0, 149.0, 148.4, 148.6, 141.35, 137.3, 134.4, 129.1, 128.2, 122.6, 121.9, 119.9, 119.5, 114.2, 112.7, 110.9, 107.4, 102.6, 56.3, 33.2. ESI-Mass m/z: 391 [M + H]$^+$. Anal. calcd. for $C_{21}H_{18}N_4O_4$: C, 64.61, H, 4.56; N, 14.35. Found: C, 64.30; H, 4.82; N, 14.72.

N′-(2-Fluorobenzylidene)-5-(1-methyl-1*H*-indol-3-yl)isoxazole-3-carbohydrazide (5h)

Yield: 64%; cream-white solid; m.p. 258–260 ℃. ^{1}H NMR(400 MHz, DMSO-d_6): δ 11.92 (s, 1H, CONH), 8.81 (s, 1H, −N = CH−), 7.98 (t, 1H, J = 8.0 Hz, −N = CH−C_6H_5 H_4), 7.91 (d, 1H, J = 8.0 Hz, −N = CH−C_6H_5 H_6), 7.85 (s, 1H, Indole H_2), 7.56–7.49 (m, 2H, Indole H_4, H_7), 7.33- 7.27 (m, 3H, −N = CH−C_6H_5 H_3, H_5, Indole H_5), 7.21 (t, 1H, J = 8.0 Hz, Indole H_6), 7.07 (s, 1H, Isoxazole), 3.88 (s, 3H, N−CH_3). ^{13}C NMR (100 MHz, DMSO-d_6):168.3 (d, J_{C-F} = 245.3 Hz), 168.1, 160.0, 159.1, 149.9, 146.5, 140.2 (d, J_{C-F} = 8.0 Hz), 139.2, 137.3, 132.2 (d, J_{C-F} = 8.0 Hz), 128.4, 126.8, 125.4, 122.5, 120.7, 119.7 (d, J_{C-F} = 21.5 Hz), 116.8 (d, J_{C-F} = 21.0 Hz), 110.9, 102.6, 33.4. ESI-Mass m/z: 363 [M + H]$^+$. Anal. calcd. for $C_{20}H_{15}FN_4O_2$: C, 66.29, H, 4.17; N, 15.46. Found: C, 66.51; H, 4.25; N, 15.83.

N′-(2-Chlorobenzylidene)-5-(1-methyl-1*H*-indol-3-yl)isoxazole-3-carbohydrazide (5i)

Yield: 72%; off-white solid; m.p. 280–283 ℃. ^{1}H NMR (400 MHz, DMSO-d_6): δ 12.06 (s, 1H, CONH), 8.97 (s, 1H, −N = CH−), 8.05 (s, 1H, −N = CH−C_6H_5 H_3), 7.90 (d, 1H, J = 8.0 Hz, −N = CH−C_6H_5 H_6), 7.84 (s, 1H, Indole H_2), 7.56- 7.53 (m, 2H, Indole H_4, H_7), 7.46 (m, 2H, −N = CH−C_6H_5 H_4, H_5), 7.28 (t, 1H, J = 8.0 Hz, Indole H_5),

7.21 (t, 1H, $J = 8.0$ Hz, Indole H$_6$), 7.08 (s, 1H, Isoxazole), 3.88 (s, 3H, N−CH$_3$). ^{13}C NMR (100 MHz, DMSO-d_6): 159.0, 146.6, 143.5, 139.3, 137.3, 134.9, 132.8, 131.8, 131.4, 128.9, 128.4, 126.0, 125.1, 122.6, 120.7, 119.8, 110.9, 104.0, 102.6, 33.3. ESI-Mass m/z: 379 [M + H]$^+$. Anal. calcd. for C$_{20}$H$_{15}$ClN$_4$O$_2$: C, 63.41, H, 3.99; N, 14.79. Found: C, 63.73; H, 4.06; N, 14.51.

N′-(3-Bromobenzylidene)-5-(1-methyl-1*H*-indol-3-yl)isoxazole-3-carbohydrazide (5j)
Yield: 52%; off-white solid; m.p. 152–157 ℃. ^{1}H NMR (400 MHz, DMSO-d_6): δ 11.87 (s, 1H, CONH), 8.52 (s, 1H, −N═CH−), 7.91–7.90 (m, 2H, Indole H$_4$, −N═CH−C$_6$H$_4$ H$_2$), 7.85 (s, 1H, Indole H$_2$), 7.70 (d, 1H, $J = 8.0$ Hz, −N═CH−C$_6$H$_4$ H$_4$), 7.64 (d, 1H, $J = 8.0$ Hz, Indole H$_7$), 7.56 (d, 1H, $J = 8.0$ Hz, −N═CH−C$_6$H$_4$ H$_6$), 7.44 (t, 1H, $J = 8.0$ Hz, −N═CH−C$_6$H$_4$ H$_5$), 7.29 (t, 1H, $J = 8.0$ Hz, Indole H$_5$), 7.21 (t, 1H, $J = 8.0$ Hz, Indole H$_6$), 7.07 (s, 1H, Isoxazole H$_4$), 3.88 (s, 3H, CH$_3$). ^{13}C NMR (100 MHz, DMSO-d_6): 168.2, 158.8, 155.0, 145.7, 139.8, 137.9, 137.8, 131.5, 128.0, 126.7, 126.1, 125.1, 124.7, 122.7, 120.8, 120.7, 110.5, 102.6, 101.2, 33.7. ESI-Mass m/z: 424 [M + H]$^+$. Anal. calcd. for C$_{20}$H$_{15}$BrN$_4$O$_2$: C, 56.75, H, 3.57; N, 13.24. Found: C, 56.89; H, 3.29; N, 13.44.

N′-(3-Nitrobenzylidene)-5-(1-methyl-1*H*-indol-3-yl)isoxazole-3-carbohydrazide (5k)
Yield: 64%; yellow solid; m.p. 268–270 ℃. ^{1}H NMR (400 MHz, DMSO-d_6): δ 11.99 (s, 1H, CONH), 8.66 (s, 1H, −N=CH−), 8.53 (s, 1H, −N=CH−C$_6$H$_5$ H$_2$), 8.27 (d, 1H, $J = 8.0$ Hz, −N=CH−C$_6$H$_5$ H$_4$), 8.14 (d, 1H, $J = 8.0$ Hz, −N=CH−C$_6$H$_5$ H$_6$), 7.90 (d, 1H, $J = 8.0$ Hz, Indole H$_4$), 7.84 (s, 1H, Indole H$_2$), 7.77 (t, 1H, $J = 8.0$ Hz, −N=CH−C$_6$H$_5$ H$_5$), 7.55 (d, 1H, $J = 8.0$ Hz, Indole H$_7$), 7.28 (t, 1H, $J = 8.0$ Hz, Indole H$_5$), 7.22 (t, 1H, $J = 8.0$ Hz, Indole H$_4$), 7.08 (s, 1H, Isoxazole), 3.88 (s, 3H, N−CH$_3$). ^{13}C NMR (100 MHz, DMSO-d_6): 168.8, 159.8, 159.1, 148.7, 146.3, 136.4, 134.5, 131.1, 128.4, 125.1, 122.2, 120.7, 119.8, 119.7, 110.9, 108.7, 102.7, 100.1, 99.2, 33.3. ESI-Mass m/z: 390 [M + H]$^+$. Anal. calcd. for C$_{20}$H$_{15}$N$_5$O$_4$: C, 61.69, H, 3.88; N, 17.99. Found: C, 61.61; H, 4.13; N, 17.69.

N′-(4-(Methylthio)benzylidene)-5-(1-methyl-1*H*-indol-3-yl)isoxazole-3-carbohydrazide (5l)
Yield: 54%; light-gray solid; m.p. 254–255 ℃. ^{1}H NMR (400 MHz, DMSO-d_6): δ 8.50 (s, 1H, CONH), 8.10 (bs, 1H, −N=CH−), 7.89–7.83 (m, 2H, Indole H$_2$, H$_4$), 7.66–7.54 (m, 3H, Indole H$_5$, H$_6$, H$_7$), 7.34–7.22 (m, 4H, −N=CH−C$_6$H$_5$ H$_2$, H$_3$, H$_5$, H$_6$), 7.05 (s, 1H, Isoxazole), 3.87 (s, 3H, N−CH$_3$), 2.37 (s, 3H, CH$_3$). ^{13}C NMR (100 MHz, DMSO-d_6): 169.9, 160.0, 154.5, 152.7, 142.7, 138.8, 134.8, 130.2, 128.9, 128.0, 127.4, 120.9, 119.9, 116.6, 113.0, 110.1, 106.4, 102.8, 98.3, 33.9, 14.7. ESI-Mass m/z: 391 [M + H]$^+$. Anal. calcd. for C$_{21}$H$_{18}$N$_4$O$_2$S: C, 64.60, H, 4.65; N, 14.35. Found: C, 64.75; H, 4.73; N, 14.54.

5-(1-Methyl-1*H*-indol-3-yl)-N′-((pyridin-4-yl)methylene)isoxazole-3-carbohydrazide (5m)
Yield: 75%; light-brown solid; m.p. 225–227 ℃. ^{1}H NMR (400 MHz, DMSO-d_6): δ 9.39 (s, 1H, CONH), 8.58 (bs, 1H, −N=CH−), 7.92- 7.67 (m, 4H, Indole H$_4$, H$_7$, Pyr. H$_3$, H$_5$), 7.51 (d, 2H, $J = 8.0$ Hz, −N=CH−Pyr. H$_2$, H$_6$), 7.24 (t, 1H, $J = 8.0$ Hz, Indole H$_5$), 7.16 (t, 1H, $J = 8.0$ Hz, Indole H$_6$), 7.08–6.99 (m, 2H, Isoxazole, Indole H$_2$), 3.89 (s, 3H, N−CH$_3$). ^{13}C NMR (100 MHz, DMSO-d_6): 169.9, 158.6, 154.1, 151.9, 148.9, 141.0, 137.3, 136.2, 131.7, 127.9, 122.0, 120.0, 118.3, 115.1, 112.8, 110.5, 101.6, 100.0, 33.1. ESI-Mass m/z: 346 [M + H]$^+$. Anal. calcd. for C$_{19}$H$_{15}$N$_5$O$_2$: C, 66.08, H, 4.38; N, 20.28. Found: C, 65.75; H, 4.39; N, 20.60.

In vitro cholinesterase inhibitory activity
The anti-cholinesterase activity of synthesized compounds was performed according to our previous study[32,33].

Kinetic characterization of AChE inhibition
To elucidate the mechanism of action of compound **5d**, reciprocal plots of 1/velocity versus 1/[substrate] were conducted using Ellman's method. The substrate, acetylthiocholine, was tested at different concentrations (187.5, 750, 1500 and 3000 µM). In the assay, various concentrations of compound **5d** (0, 13.36, 53.47 and 106.95 µM) were introduced into the reaction mixture, which was then preincubated with the enzyme at room temperature for 10 min before adding the substrate. Kinetic measurements were recorded at 412 nm while monitoring the enzyme catalyzed reaction. A parallel control experiment was conducted without the presence of the inhibitor[34].

BACE1 inhibitory activity
The investigation of the inhibitory activity of the selected compounds was performed using a FRET-based assay kit provided by Invitrogen (previously known as Pan Vera, Madison, WI). As a reference inhibitor, OM99-2 was employed. Detailed information on the methodology can be found in our previously published studies[28,35].

Metal Chelating Activity
Metal binding studies were conducted using an Agilent UV-2450 spectrophotometer in a 1 cm quartz cuvette, employing the mole ratio method. Investigating the metal binding capability of the chosen derivative involved recording the UV absorption of the **5d** (dissolved in MeOH) with and without Fe^{3+} ions in the solution. The UV absorption was measured within the wavelength range of 200 to 600 nm after incubation at room temperature for 30 min. All substances were dissolved in absolute methanol, with the **5d** concentration set at 20 µM and the Fe^{3+} concentration varying from 0 to 50 µM. The stoichiometry of the complex was determined by gradually adding FeCl$_3$ to the methanol solution of the tested compound.

Molecular docking
The molecular docking of the synthesized molecules was conducted using the Schrödinger Suites Maestro molecular modeling platform[36]. X-ray crystallographic structures of AChE and BACE1 were obtained from the

RCSB Protein Data Bank (www.rcsb.org), with PDB IDs of 4EY7 and 1W51, respectively[37]. The protein preparation wizard was used to remove co-crystallized atoms and water molecules from the proteins to construct the protein structures[38]. The prime tool was used to add any missing loops, and the terminals were then sealed[39]. Additionally, pH 7.4 was used to create hetero atom states using EPIK, and pH 7.4 was used to assign H-bonding interactions using PROPKA. ChemDraw (ver. 16) was used to create the 2D structures of the ligands, which were then exported as SDF files. The SDF files were created using the OPLS3e force field and the ligand preparation wizard. Using an induced-fit docking approach[40], the interactions of the ligands were studied. The receptor and ligand's van der Waals radii were set at 0.7 and 0.5, respectively.

Molecular dynamics simulations

The starting model was obtained by imposing the induced fit docking to BACE1 (PDB ID: 1W51) and AChE (4EY7). MD simulations were conducted using the Desmond v5.3 of Schrodinger's suit maestro according to previously reported procedures[41,42].

Data availability

References

1. Sanders, O. & Rajagopal, L. Phosphodiesterase inhibitors for Alzheimer's disease: A systematic review of clinical trials and epidemiology with a mechanistic rationale. *J. Alzheimers Dis. Rep.* **4**, 185–215 (2020).
2. Breijyeh, Z. & Karaman, R. Comprehensive review on Alzheimer's disease: Causes and treatment. *Molecules* **25**, 5789 (2020).
3. Kocahan, S. & Doğan, Z. Mechanisms of Alzheimer's disease pathogenesis and prevention: The brain, neural pathology, N-methyl-D-aspartate receptors, tau protein and other risk factors. *Clin. Psychopharmacol. Neurosci.* **15**, 1–8 (2017).
4. Puzzo, D. *et al.* Phosphodiesterase 5 inhibition improves synaptic function, memory, and amyloid-β load in an Alzheimer's disease mouse model. *J. Neurosci.* **29**, 8075–8086 (2009).
5. Hamulakova, S. *et al.* Design and synthesis of novel tacrine–indole hybrids as potential multitarget-directed ligands for the treatment of Alzheimer's disease. *Future Med. Chem.* **13**, 785–804 (2021).
6. Guzior, N., Wieckowska, A., Panek, D. & Malawska, B. Recent development of multifunctional agents as potential drug candidates for the treatment of Alzheimer's disease. *Curr. Med. Chem.* **22**, 373–404 (2015).
7. Pourtaher, H., Hasaninejad, A., Zare, S., Tanideh, N. & Iraji, A. The anti-Alzheimer potential of novel spiroindolin-1,2-diazepine derivatives as targeted cholinesterase inhibitors with modified substituents. *Sci. Rep.* **13**, 11952 (2023).
8. Pourtaher, H., Hasaninejad, A. & Iraji, A. Design, synthesis, in silico and biological evaluations of novel polysubstituted pyrroles as selective acetylcholinesterase inhibitors against Alzheimer's disease. *Sci. Rep.* **12**, 15236 (2022).
9. Evin, G. & Hince, C. BACE1 as a therapeutic target in Alzheimer's disease: Rationale and current status. *Drugs Aging* **30**, 755–764 (2013).
10. Vassar, R. & Kandalepas, P. C. The β-secretase enzyme BACE1 as a therapeutic target for Alzheimer's disease. *Alzheimers Res. Ther.* **3**, 20 (2011).
11. Oliyaei, N., Moosavi-Nasab, M., Tanideh, N. & Iraji, A. Multiple roles of fucoxanthin and astaxanthin against Alzheimer's disease: Their pharmacological potential and therapeutic insights. *Brain Res Bull.* **193**, 11–21 (2023).
12. Zeng, W. *et al.* Indole-containing pharmaceuticals: Targets, pharmacological activities, and SAR studies. *RSC Med. Chem.* **15**, 788–808 (2024).
13. Taha, M. *et al.* Exploring indole-based-thiadiazole derivatives as potent acetylcholinesterase and butyrylcholinesterase enzyme inhibitors. *Int. J. Biol. Macromol.* **188**, 1025–1036 (2021).
14. Iraji, A. *et al.* Design, synthesis, spectroscopic characterization, in vitro tyrosinase inhibition, antioxidant evaluation, in silico and kinetic studies of substituted indole-carbohydrazides. *Bioorg. Chem.* **129**, 106140 (2022).
15. Li, Y. *et al.* Synthesis, antibacterial activity, and 3D-QASR studies of matrine-indole derivatives as potential antibiotics. *Bioorg. Med. Chem. Lett.* **102**, 129671 (2024).
16. Sifaoui, I. *et al.* Amoebicidal effect of synthetic indoles against Acanthamoeba spp.: a study of cell death. *Antimicrob. Agents Chemother.* **68**, e01651-e11623 (2024).
17. Kaur, K., Verma, H., Gangwar, P., Dhiman, M. & Jaitak, V. Design, Synthesis, in vitro and in silico evaluation of indole based tetrazole derivatives as putative anti-breast cancer agent. *RSC Med. Chem.* **15**, 1329 (2024).
18. George, N., Jawaid Akhtar, M., Al Balushi, K. A. & Alam Khan, S. Rational drug design strategies for the development of promising multi-target directed indole hybrids as anti-Alzheimer agents. *Bioorg. Chem.* **127**, 105941 (2022).
19. Konopelski, P. & Mogilnicka, I. Biological effects of indole-3-propionic acid, a gut microbiota-derived metabolite, and its precursor tryptophan in mammals' health and disease. *Int. J. Mol. Sci.* **23**, 1222 (2022).
20. Mallik, N. N. *et al.* Synthesis of fused isoxazoles: A comprehensive review. *Eng. Proc.* **59**, 222 (2024).
21. Koufaki, M. *et al.* Isoxazole substituted chromans against oxidative stress-induced neuronal damage. *Bioorg. Med. Chem.* **19**, 4841–4850 (2011).
22. Shaik, A. *et al.* Antimicrobial, antioxidant, and anticancer activities of some novel isoxazole ring containing chalcone and dihydropyrazole derivatives. *Molecules* **25**, 1047 (2020).
23. Filali, I., Romdhane, A., Znati, M., Jannet, B. H. & Bouajila, J. Synthesis of new harmine isoxazoles and evaluation of their potential anti-alzheimer, anti-inflammatory, and anticancer activities. *Med. Chem.* **12**, 184–190 (2016).
24. Saeedi, M. *et al.* Design and synthesis of novel arylisoxazole-chromenone carboxamides: Investigation of biological activities associated with Alzheimer's disease. *Chem. Biodivers.* **17**, e1900746 (2020).
25. Saeedi, M. *et al.* Novel N′-substituted benzylidene benzohydrazides linked to 1, 2, 3-triazoles: potent α-glucosidase inhibitors. *Sci. Rep.* **13**, 8960 (2023).
26. Yar, M. *et al.* Design and Synthesis of New Dual Binding Site Cholinesterase Inhibitors: in vitro Inhibition Studies with in silico Docking. *Lett. Drug Des. Discov.* **11**, 331–338 (2014).
27. Parveen, S. *et al.* Modification of Bischler-Möhlau indole derivatives through palladium catalyzed Suzuki reaction as effective cholinesterase inhibitors, their kinetic and molecular docking studies. *Bioorg. Chem.* **76**, 166–176 (2018).

28. Iraji, A. *et al.* Synthesis and structure-activity relationship study of multi-target triazine derivatives as innovative candidates for treatment of Alzheimer's disease. *Bioorg. Chem.* **77**, 223–235 (2018).

29. Iraji, A. *et al.* Multifunctional iminochromene-2H-carboxamide derivatives containing different aminomethylene triazole with BACE1 inhibitory, neuroprotective and metal chelating properties targeting Alzheimer's disease. *Eur. J. Med. Chem.* **141**, 690–702 (2017).

30. Agrawal, N. & Mishra, P. The synthetic and therapeutic expedition of isoxazole and its analogs. *Med. Chem. Res.* **27**, 1309–1344 (2018).

31. Vafadarnejad, F. *et al.* Novel indole-isoxazole hybrids: synthesis and in vitro anti-cholinesterase activity. *Lett. Drug Des. Discov* **14**, 712–717 (2017).

32. Najafi, Z. *et al.* Novel tacrine-coumarin hybrids linked to 1,2,3-triazole as anti-Alzheimer's compounds: In vitro and in vivo biological evaluation and docking study. *Bioorg. Chem.* **83**, 303–316 (2019).

33. Karimi Askarani, H. *et al.* Design and synthesis of multi-target directed 1,2,3-triazole-dimethylaminoacryloyl-chromenone derivatives with potential use in Alzheimer's disease. *BMC Chem.* **14**, 64 (2020).

34. Saeedi, M. *et al.* Design and Synthesis of Selective Acetylcholinesterase Inhibitors: Arylisoxazole-Phenylpiperazine Derivatives. *Chem. Biodivers.* **16**, e1800433 (2019).

35. Edraki, N. *et al.* N-(2-(Piperazin-1-yl) phenyl) arylamide derivatives as β-secretase (BACE1) inhibitors: Simple synthesis by Ugi four-component reaction and biological evaluation. *Arch. Pharm.* **348**, 330–337 (2015).

36. Schrödinger Suite 2018, Induced Fit Docking protocol; Glide Version 5.5, S., LLC, New York, NY, 2009; Prime Version 2.1, Schrödinger, LLC, New York, NY, 2009.

37. Saeedi, M. *et al.* Cinnamomum verum J. Presl. Bark essential oil in vitro investigation of anti-cholinesterase, anti-BACE1, and neuroprotective activity. *BMC Complement Med. Ther.* **22**, 303 (2022).

38. Schrödinger Release 2018–4: Schrödinger Release 2018–4 Protein Preparation Wizard; Epik, Schrödinger, LLC, New York, NY, 2016; Impact, Schrödinger, LLC, New York, NY, 2016; Prime, Schrödinger, LLC, New York, NY, 2019.

39. Schrödinger Release 2018–4: Induced Fit Docking Protocol; Glide, Schrödinger, LLC, New York, NY, 2018; Prime, Schrödinger, LLC, New York, NY, 2018.

40. Schrödinger LLC . Schrödinger Release 2018–4: LigPrep. Schrödinger LLC; 2018.

41. Schrödinger LLC . Schrödinger Release 2018–4: Desmond Molecular Dynamics System, D. E. Shaw Research, New York, NY, 2018. Maestro-Desmond Interoperability Tools. Schrödinger LLC; 2018.

42. Halim, S. A. Main protease through structure-based virtual screening and molecular dynamic simulation. *Pharmaceuticals* **14**, 896. https://doi.org/10.3390/ph14090896 (2021).

Acknowledgements

Author contributions

"A.I. and M.N.M. performed in silico study and contributed to the preparation of the article; P.N., M.K. synthesized compounds and contributed to the characterization of compounds. S.S.M. supervised the chemistry part of the study. N.E. performed BACE1 and metal chelation assay. MS. supervised the AChE and BuChE biological assay. All authors read and approved the final version of the article".

Competing interests

The authors declare no competing interests.

Additional information

Supplementary Information The online version contains supplementary material available at https://doi.org/10.1038/s41598-024-71729-0.

Correspondence and requests for materials should be addressed to M.S. or S.S.M.

Reprints and permissions information is available at www.nature.com/reprints.

Publisher's note Springer Nature remains neutral with regard to jurisdictional claims in published maps and institutional affiliations.